Contribution of multiple electron rescatterings on high-order harmonic generation in the mid-infrared wavelength regime

Xiaolong Yuan (袁晓龙)[1,3]**, Candong Liu (刘灿东)**[1,*]**, Pengfei Wei (尉鹏飞)**[2,**]**,
Zhinan Zeng (曾志男)[1,***]**, and Ruxin Li (李儒新)**[1]

[1]*State Key Laboratory of High Field Laser Physics, Shanghai Institute of Optics and Fine Mechanics,*
Chinese Academy of Sciences, Shanghai 201800, China
[2]*Department of Physics, Shaoxing University, Shaoxing 312000, China*
[3]*University of Chinese Academy of Sciences, Beijing 100039, China*
*Corresponding author: cdliu@siom.ac.cn; **corresponding author: pfwei@usx.edu.cn;
***corresponding author: zhinan_zeng@mail.siom.ac.cn

We theoretically investigate multiple electron rescatterings in high-order harmonic generation with a wide range of driving laser wavelengths. In order to obtain a clear and intuitive insight, the time-frequency analysis of the dipole acceleration calculated by the numerical solution of the time-dependent Schrödinger equation is performed and compared with the classical electron trajectory calculation. The result shows that in the mid-infrared regime, the high-order electron trajectory associated with multiple rescatterings plays a more important role than the usually referred-to "long and "short" electron trajectories. To provide quantitative evidence, the strong-field approximation is used to calculate the yield ratio of the high-order harmonic generation from the first rescattering and the multiple rescatterings.

OCIS codes: 020.2649, 190.2620, 320.2250, 320.7110.
doi: 10.3788/COL201614.030201.

High-order harmonic generation (HHG) and its application in the production of attosecond pulses have been extensively investigated in recent years[1–3]. In the HHG process, the semi-classical three-step model predicts the maximum photon energy equal to $3.17U_p + I_p$, where I_p is the ionization potential of the target gas and U_p is the ponderomotive energy that is proportional to the square of the wavelength of the driving pulse. The cut-off law shows that the use of a longer wavelength will greatly extend the maximal harmonic photon energy. Recently, the rapid development of ultrafast laser technology has enabled the generation of high-power femtosecond laser pulses at mid-infrared wavelengths, which has further stimulated the study of HHG in the mid-infrared wavelength regime[4–8]. It has been commonly accepted that the spreading of the returning wave packet would result in a λ^{-3} dependence of the HHG efficiency[9] as long as the ground-state depletion can be neglected[10]. However, a more rapid decrease in the HHG yields scaling: $\lambda^{-5\sim-6}$ has been found by solving the time-dependent Schrödinger equation (TDSE) for argon and by using the strong-field approximation (SFA) for helium[11]. A further work has shown that the harmonic yield does not smoothly decrease with the fundamental wavelength, but exhibits the rapid oscillations with a period of 6–20 nm depending on the wavelength region[12,13]. With the analytical theory for a short-range potential model, the oscillations on the fine λ scale can be explained as the threshold phenomena, and the wavelength scaling of $\lambda^{-5} \sim \lambda^{-6}$ has been confirmed

again[14]. Interestingly, using the mid-infrared laser pulses, a regular wave form on the zeptosecond time scale has been predicted, which can be explained by the interference of high-harmonic emission from multiple electron rescatterings[15]. Most recently, the quantum trajectory analysis for HHG with different driving laser wavelengths and the ratio of HHG yields of the Nth and the first rescattering event has been investigated by the SFA[16]. The considering wavelengths do not exceed 2000 nm in many previous works[11–14,16].

In this Letter, we theoretically investigate the multiple electron rescatterings during HHG in the mid-infrared wavelength regime. The classical model is firstly employed to analyze the electron trajectory due to its advantage of providing a clear physical picture and deep insights into the time-frequency analysis of the dipole acceleration obtained from the TDSE. By comparing classical electron trajectories with the results of the time-frequency analysis, one can see that the multiple rescatterings play a more important role in the mid-wavelength regime. The results agree well with those in the Refs. [11,16]. Especially in the case of a driving laser wavelength greater than 2400 nm, we found that the contribution of the first electron rescattering to the HHG cannot be found in the time-frequency analysis, and the effect of multiple electron rescatterings will play a more and more important role. In order to distinguish the contributions from the first rescattering and the multiple rescatterings quantitatively, we calculate the

relative yield ratio of the first rescattering and the multiple rescatterings by using the SFA.

Firstly, the classical model is used to simulate the HHG process, which considers the electron rescattering from the nuclei several times. The time of the electron recombining to the parent core is restricted to one fixed laser period. For this reason, we define these electrons ionized at each half cycle before the recombining period as $n = 1, 2...$, as shown in Fig. 1(a). In this classical model, the recombining time and the corresponding ionization time are denoted as t_r and t_i, respectively. For a given trajectory, t_r and t_i can be estimated by solving the following equation[17]:

$$0 = x(t_i) - x(t_r) = \int_{t_i}^{t_r} \int_{t_i}^{t} E(t')\mathrm{d}t'\mathrm{d}t, \quad (1)$$

where, $x(t)$ is the time-dependent electron trajectory, and $E(t)$ is the electric field of the driving laser. We calculate the kinetic energy based on Newtonian mechanics without considering the ionizing time or the Coulomb field.

The maximum kinetic energy of the rescattering electrons as a function of n is shown in Fig. 1(b). Although only four cycles described in our definition are shown in Fig. 1, n can be very large for a multi-cycle laser pulse. As described by previous research[18–20], the maximum kinetic energy is about $3.17U_p$ for the first return ($n = 1$). However, the maximum kinetic energy is close to $2U_p$ when n gradually increases. Compared with the case of the first return, this trend indicates that a different mechanism for multiple rescatterings exists.

In order to obtain more information, for a different rescattering trajectory, we check the electric field value at those moments when the electron is ionized. For different n, the electric field corresponding to ionization time t_i is plotted as a function of the rescattering time t_r, as shown in the Fig. 2. One can see that all the electrons of $n > 1$ are ionized around the crest of the electric field where the electric field is very close to the maximum. According to the Ammosov-Delone-Krainov (ADK) model[21], the ionization rate exponentially depends on the electric field,
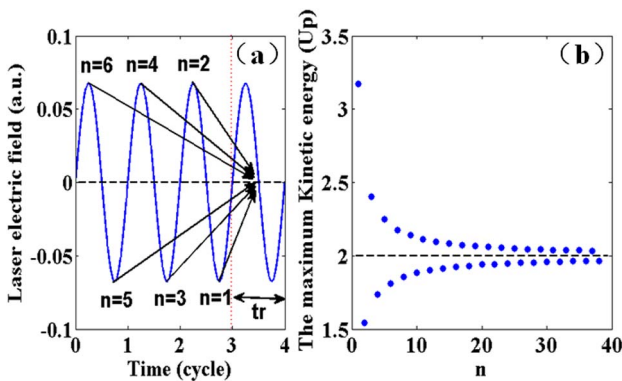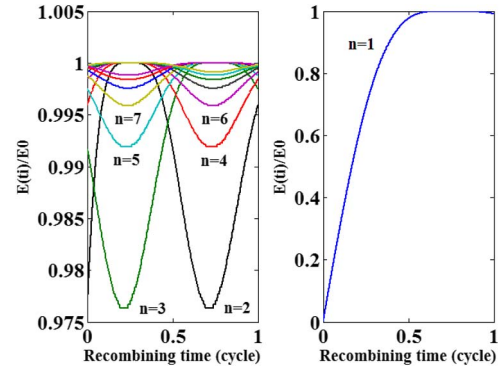
Fig. 2. Electric fields corresponding to ionization time t_i as functions of the rescattering time t_r for different n.

which means that tunneling ionizations corresponding to multiple rescatterings happens within a very small fraction of an optical cycle. Therefore, the tunneling processes of all the electrons of $n > 1$ are completed in a shorter time than the first return ($n = 1$). In strong-field science, tunnel ionization through the barrier formed by the external laser field and the Coulomb potential is the first step that triggers the subsequent dynamics. For this reason, multiple rescatterings correspond to different dynamics in the mid-infrared regime.

Second, the classical model gives the above result independent of the wavelength of the laser pulse. To investigate the influence of wavelength, we calculate the dipole acceleration for different wavelengths by solving the TDSE within the single-active electron approximation (SAE) numerically. Atomic units are used in the work. The Schrödinger equation can be written as

$$i\frac{\partial\Psi(\vec{x}, t)}{\partial t} = \left[-\frac{1}{2}\nabla^2 + V(x) + \vec{x} \cdot \vec{F}(t)\right]\Psi(\vec{x}, t), \quad (2)$$

where $F(t) = f(t)F_0 \sin(\omega t)$, $f(t)$, and $V(x)$ denote the laser electric field, the envelope function and, the atomic potential, respectively. $f(t)$ is chosen as the trapezoid envelope that rises linearly from zero to one during the first half-optical cycle, then holds constant for five optical cycles, and then decreases linearly from one to zero during the last half-optical cycle. This particular choice of $f(t)$ cannot affect the nature of the physical reality[12]. The model of the Coulomb potential for argon was used in our simulation[22]. In order to propagate the time-dependent wave function efficiently, we choose the second-order split-operator method[23]. The imaginary time propagation scheme allows us to obtain the wave function of the ground state. The wave function is multiplied by a $\cos^{1/8}$ mask function in order to avoid any spurious reflection of the wave packet from the boundary. The simulation parameters used in our TDSE calculation are as follows: the radial grid contains 16384 points with a step of $\mathrm{d}x = 0.1$ a.u., and 2048 mesh points in one optical cycle are used for three different laser wavelengths (800, 1600, and 2400 nm). To explore the detailed spectral and

Fig. 1. (a) The schematic of the definition of multiple rescatterings. (b) The maximum kinetic energy of the rescattering electrons as a function of n.

temporal structures of the HHG, we performed the time-frequency analysis by means of the wavelet transform of the induced dipole acceleration by calculating the following equation[24]:

$$A_w(t_0, \omega) = \int d(t) w_{t_0,\omega}(t) \mathrm{d}t = \int d(t) \sqrt{\omega} \, W(\omega(t - t_0)) \mathrm{d}t. \tag{3}$$

For the harmonics emission, we choose the Morlet wavelet and the parameter $\tau = 15$ to perform the wavelet transform[18]. The Morlet wavelet equation can be written as

$$W(x) = (1/\sqrt{\tau}) e^{ix} e^{-x^2/2\tau^2}. \tag{4}$$

The results of the time-frequency analysis that was applied are shown in Figs. 3(a)–3(c). In previous works[12,13], the high-order harmonics of photon energy between 20 and 50 eV were considered; these are also included in our work. For a direct comparison, we set the same laser intensity and profile for different wavelengths. When the laser intensity is 1.6×10^{14} W/cm², the corresponding ponderomotive energies U_p for 800, 1600, and 2400 nm are 9.5 eV (0.35 a.u.), 38.2 eV (1.41 a.u.), and 85.85 eV (3.16 a.u.), respectively. The range of 20 to 50 eV belongs to a different region because the value of U_p is different for different laser wavelengths. The value of 50 eV is almost $3.17 U_p$ for the 800 nm wavelength, but the value of 50 eV is only about $0.13 U_p$ for the 2400 nm wavelength. The corresponding classical results of the 800, 1600, and 2400 nm are shown in the Figs. 3(d)–3(f), respectively. In order to achieve a direct comparison, the ionization potential is subtracted in our time-frequency analysis to get the kinetic energy, $E_k = (E - I_p)/U_p$. From Fig. 3, one can see that all the results calculated by solving the TDSE agree well with the classical calculation results. From these comparisons, the most important conclusion is that the main contribution for the HHG is from $n > 1$ electrons for the long-wavelength laser pulse. When the wavelength
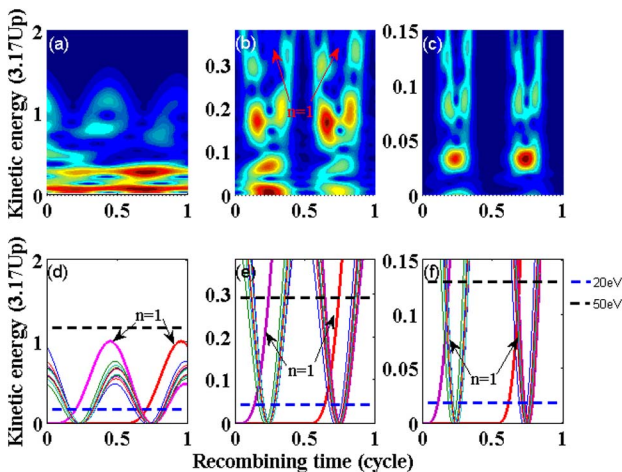

Fig. 3. Time-frequency analysis of the dipole acceleration for (a) 800, (b) 1600, and (c) 2400 nm. (d)–(f) The corresponding classical calculation for the three different wavelengths.

of the laser pulse is 1600 nm, the contribution of the $n = 1$ electron can still be seen. But when the wavelength is increased to be 2400 nm, the $n = 1$ contribution cannot be resolved in the result obtained from the time-frequency analysis, and the higher-order returns have surprisingly large amplitudes in the fixed photo-energy region. Because the short path of the first rescattering plays an important role in the wavelength-dependent HHG yield ratios[16], the phase matchings of the short trajectory of the first rescattering are mainly considered in general experiments. Consequently, the increasing effect of the multiple scatterings and the $n = 1$ short trajectory disappearing decrease the macroscopic efficiency in the mid-infrared wavelength regime.

Finally, the TDSE simulation is the most precise method to compute the HHG yield, but it is impossible to separate the multiple scatterings. The alternative Lewenstein model[9] is used to calculate the harmonic radiation in the single-atom response to give us more evidence. Based on the saddle-point method, the time-dependent dipole can be expressed as:

$$\vec{r}(t) = i \int_0^\infty \mathrm{d}\tau \left(\frac{\pi}{\varepsilon + i\tau/2} \right)^{3/2} \vec{d}^*[\vec{p}_s(t,\tau) - \vec{A}(t)] g^*(t) e^{iS(\vec{p}_s,t,\tau)}$$
$$\bullet \, \vec{F}(t - \tau) \vec{d}[\vec{p}_s(t,\tau) - \vec{A}(t - \tau)] g(t) + \text{c.c.}, \tag{5}$$

where t and t' are the recombination time and the ionization time, yielding $\tau = t - t'$, and $g(t)$ is the ground-state depletion, which can be calculated by the ADK[21] tunneling model. In this equation, $d(p)$ is the notation of a dipole transition matrix element from the ground state to the continuum state. In our simulation, we approximately calculate $d(p)$ by

$$\vec{d}_{1s}(\vec{p}) = i \frac{2^{7/2}}{\pi} I_p^{5/4} \frac{\vec{p}}{(\vec{p}^2 + I_p)^3}. \tag{6}$$

The specific calculation methods of the stationary momentum P_s and the quasi-classical action S are described in Ref. [9]. Since the electron excursion time associated with the first rescattering is less than one optical cycle (T_0), the contributions of the first rescattering and high-order rescatterings can be distinguished by the following division of the time-dependent dipole moment:

$$\vec{r}(t) = \int_0^{T_0} \vec{r}(t') \mathrm{d}t' + \int_{T_0}^\infty \vec{r}(t') \mathrm{d}t', \tag{9}$$

where the first term represents the first rescattering and the second term represents the high-order rescattering.

We define the relative HHG yield ratio as $R = Y_2/Y_1$, where Y_1 is the HHG yield obtained from the first rescattering and Y_2 is the HHG yield obtained from the multiple rescatterings. The yield Y is calculated by integrating the harmonic yield over the range from 20 eV to $I_p + 3.17 U_p$. The driving laser is a ten-cycle flat-top pulse with one-cycle switch on and switch off. The relative HHG yield ratio as a function of the wavelength is shown in Fig. 4.
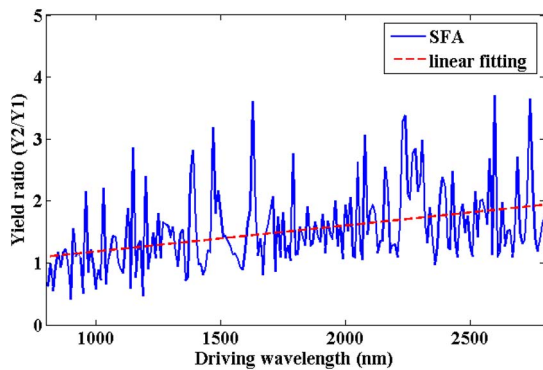
Fig. 4. Relative HHG yield ratio as a function of the driving wavelength.

One can see that the yield ratio increases with the increase of the driving wavelength and exhibits a structure of fine rapid oscillation dependent on the wavelength. The period of the fine oscillation in our simulation is consistent with the results in Ref. [13]. Although there is an oscillation structure, the linear fitting of our results shows that the general trend is rising. This rising trend of the yield ratio provides us powerful evidence that shows that multiple scatterings have more contributions with an increasing wavelength in the mid-infrared wavelength regime. We also get similar results by integrating different photon-energy ranges, although these results are not shown in this Letter.

In conclusion, we find that the maximum kinetic energy gradually approaches to $2U_p$ as the rescattering times n increase. In addition, all the electrons of $n > 1$ are ionized near the maximal position of the laser electric field. We not only see a surprising contribution of the $n > 1$ electrons in the time-frequency analysis, but also discover that the contribution of the $n = 1$ electrons cannot be resolved when the wavelength is increased to 2400 nm. By comparing the classical trajectories with the time-frequency analysis in the same photon-energy range from 20 to 50 eV, the combined effect of both multiple rescatterings and the disappearance of the $n = 1$ trajectories cause the efficiency to decrease in the mid-infrared wavelength regime. The SFA calculation gives us a more direct demonstration of the role of the multiple scatterings in the mid-infrared wavelength regime.

References

1. M. Hentschel, R. Kienberger, C. H. Spielmann, G. A. Reider, N. Milosevic, T. Brabec, P. Corkum, U. Heinzmann, M. Drescher, and F. Krausz, Nature **414**, 509 (2001).
2. Y. Mairesse, A. de Bohan, L. J. Frasinski, H. Merdji, L. C. Dinu, P. Monchicourt, P. Breger, M. Kovačev, R. Taïeb, B. Carré, H. G. Muller, P. Agostini, and P. Salières, Science **302**, 1540 (2003).
3. C. Gohle, T. Udem, M. Herrmann, J. Rauschenberger, R. Holzwarth, H. A. Schuessler, F. Krausz, and T. W. Hänsch, Nature **436**, 234 (2005).
4. B. Shan and Z. Chang, Phys. Rev. A **65**, 011804 (2001).
5. C. Vozzi, F. Calegari, F. Frassetto, L. Poletto, G. Sansone, P. Villoresi, M. Nisoli, S. De Silvestri, and S. Stagira, Phys. Rev. A **79**, 033842 (2009).
6. H. Xiong, H. Xu, Y. Fu, J. Yao, B. Zeng, W. Chu, Y. Cheng, Z. Xu, E. J. Takahashi, K. Midorikawa, X. Liu, and J. Chen, Opt. Lett. **34**, 1747 (2009).
7. T. Popmintchev, M. Chen, D. Popmintchev, P. Arpin, S. Brown, S. Ališauskas, G. Andriukaitis, T. Balčiunas, O. D. Mücke, A. Pugzlys, A. Baltuška, B. Shim, S. E. Schrauth, A. Gaeta, C. Hernández-García, L. Plaja, A. Becker, A. Jaron-Becker, M. M. Murnane, and H. C. Kapteyn, Science **336**, 1287 (2012).
8. G. Doumy, J. Wheeler, C. Roedig, R. Chirla, P. Agostini, and L. F. DiMauro, Phys. Rev. Lett. **102**, 093002 (2009).
9. M. Lewenstein, P. H. Balcou, M. Yu Ivanov, A. L'Huillier, and P. B. Corkum, Phys. Rev. A **49**, 2117 (1994).
10. A. Gordon and F. X. Kärtner, Opt. Express **13**, 2941 (2005).
11. J. Tate, T. Auguste, H. G. Muller, P. Salières, P. Agostini, and L. F. DiMauro, Phys. Rev. Lett. **98**, 013901 (2007).
12. K. Schiessl, K. L. Ishikawa, E. Persson, and J. Burgdörfer, Phys. Rev. Lett. **99**, 253903 (2007).
13. K. L. Ishikawa, K. Schiessl, E. Persson, and J. Burgdörfer, Phys. Rev. A **79**, 033411 (2009).
14. M. V. Frolov, N. L. Manakov, and A. F. Starace, Phys. Rev. Lett. **100**, 173001 (2008).
15. C. Hernández-García, J. A. Pérez-Hernández, T. Popmintchev, M. M. Murnane, H. C. Kapteyn, A. Jaron-Becker, A. Becker, and L. Plaja, Phys. Rev. Lett. **111**, 033002 (2013).
16. L. He, Y. Li, Z. Wang, Q. Zhang, P. Lan, and P. Lu, Phys. Rev. A **89**, 053417 (2014).
17. V. S. Yakovlev and A. Scrinzi, Phys. Rev. Lett. **91**, 153901 (2003).
18. X. M. Tong and C. D. Lin, J. Phys. B **38**, 2593 (2005).
19. P. B. Corkum, Phys. Rev. Lett. **71**, 1994 (1993).
20. J. L. Krause, K. J. Schafer, and J. L. Kulander, Phys. Rev. Lett. **68**, 3535 (1992).
21. M. V. Ammosov, N. B. Delone, and V. P. Krainov, Sov. Phys.—JETP **64**, 1191 (1986).
22. Q. Su and J. H. Eberly, Phys. Rev. A **44**, 5997 (1991).
23. M. R. Hermann and J. A. Fleck, Jr., Phys. Rev. A **38**, 6000 (1988).
24. X. M. Tong and S. I. Chu, Phys. Rev. A **61**, 021802 (2000).